JGR Earth Surface

RESEARCH ARTICLE
10.1029/2023JF007125

Relict and Modern Sediments on the Continental Shelf of the Northern South China Sea: A Reconsideration

Yuming Wang[1,2], Xiaohong Chen[1], Adam D. Switzer[3,4], Linlin Li[2], Yang Xu[2], Yukun Wang[2], and Peizhen Zhang[2]

[1]School of Civil Engineering, Guangdong Engineering Technology Research Center of Water Security Regulation and Control for Southern China, Sun Yat-sen University, Guangzhou, China, [2]Guangdong Provincial Key Lab of Geodynamics and Geohazards, Southern Marine Science and Engineering Guangdong Laboratory (Zhuhai), School of Earth Sciences and Engineering, Sun Yat-sen University, Zhuhai, China, [3]Asian School of the Environment, Nanyang Technological University, Singapore City, Singapore, [4]Earth Observatory of Singapore, Nanyang Technological University, Singapore City, Singapore

Abstract Understanding the temporal-spatial patterns of modern and relict sediments is of importance for assessing changes in the Quaternary environment and sea-level. Sedimentological and geochemical data is presented, along with in situ shell-based accelerator mass spectrometry ^{14}C ages of 30 samples from the surface sediments on the northern shelf of the South China Sea (NSSCS). The authors' data show that the NSSCS surface sediments exhibit considerable diversity in composition. Modern sediments are primarily constrained to the NW inner shelf, which is fed by fluvial sands sourced from Coastal South China river systems and dominated by the Pearl River Estuary delivery. The transport and discharge of the terrestrial sediments to the NSSCS is highly influenced by the Guangdong Longshore Current and its secondary cyclonic eddies. Relict sediments dominated by well-sorted, medium- and coarse-grained sands were identified in the NW Shenhu and NW Dongsha areas of the outer NSSCS. The sedimentology and geochemistry of the relict sediments imply that they were deposited in a dry and cold environment either during the low sea levels of the late Pleistocene (~40 ka) or the early Holocene (~10 ka). To the east, the Taiwan Shoal and vicinity are dominated by a sand mixture, at which the relict sediments were reworked by terrigenous supply and modern hydrodynamic environment due to the compound action of the Guangdong Longshore Current, seasonal cyclones, and Kuroshio Intrusion. The present isobaths of ~−90 m in the NSSCS might be the reflective of the early Holocene coastal delta or the last glacial maximum shoreline.

Plain Language Summary Reconstructing the temporal-spatial pattern for relict sediments in shelf environments is an important way of determining the shoreline or coastal delta position during the late glacial period or the early Holocene. The largest and longest zone of the relict sediments has been traditionally suggested to be along the outer shelf of the East Asian continental margin from Malaya to Korea across the NSSCS. However, less attention has been paid to the NSSCS relict sediments despite the fact that much research has documented the sediment supply, Holocene environment, and marine resource surveys. The authors' data revealed the development of the modern sediments in the NW inner shelf and the relict sediments in the NW Shenhu and NW Dongsha areas of the NSSCS outer shelf. The relict sediments were sourced from Coastal South China and SW Taiwan, and have a distinct depositional environment in comparison with that of the modern sediments. The temporal-spatial pattern of the relict sediments suggests that the current ca. −90 m isobaths were close to the shoreline or coastal delta at the last glacial period or the early Holocene.

Key Points:

- The modern sediments preserved on the NW inner shelf of the northern South China Sea are heavily influenced by the Guangdong Longshore Current
- Relict sediments characterized by well-sorted, medium- and coarse-grained sands dominated the NW Shenhu and Dongsha areas
- The −90 m isobaths in the NSCS are in close proximity to the last glacial maximum shoreline or northern limit of the early Holocene coastal delta

Supporting Information:

Supporting Information may be found in the online version of this article.

Correspondence to:

X. Chen and P. Zhang,
eescxh@mail.sysu.edu.cn;
zhangpeizhen@mail.sysu.edu.cn

Citation:

Wang, Y., Chen, X., Switzer, A. D., Li, L., Xu, Y., Wang, Y., & Zhang, P. (2023). Relict and modern sediments on the continental shelf of the northern South China Sea: A reconsideration. *Journal of Geophysical Research: Earth Surface*, *128*, e2023JF007125. https://doi.org/10.1029/2023JF007125

Received 17 FEB 2023
Accepted 16 JUL 2023

1. Introduction

The sediments that accumulated on the current continental shelf in various environments were largely exposed due to low sea levels during the glacial maximum period of the Pleistocene epoch (e.g., Emery, 1968; McManus, 1975; Orme, 1982). The last glacial maximum (LGM) landscape was subsequently submerged in response to the rapid rise of the post-glacial sea level, creating the early Holocene coastal zone and channel-fill deposits (e.g., Orme, 1982). These sediments, deposited in an earlier environment but not yet buried on a continental shelf, can be defined as relict sediments (e.g., Emery, 1968; Swift et al., 1971) or pseudo-equilibrium sediments as they were not necessarily in equilibrium with the current environment in which they occurred (Emery, 1968; McManus, 1975). Early sea-floor surveys showed that the relict sediments were likely present in ~70% of the total area of the world's continental shelves (e.g., Emery, 1968). Thus, they are the key components

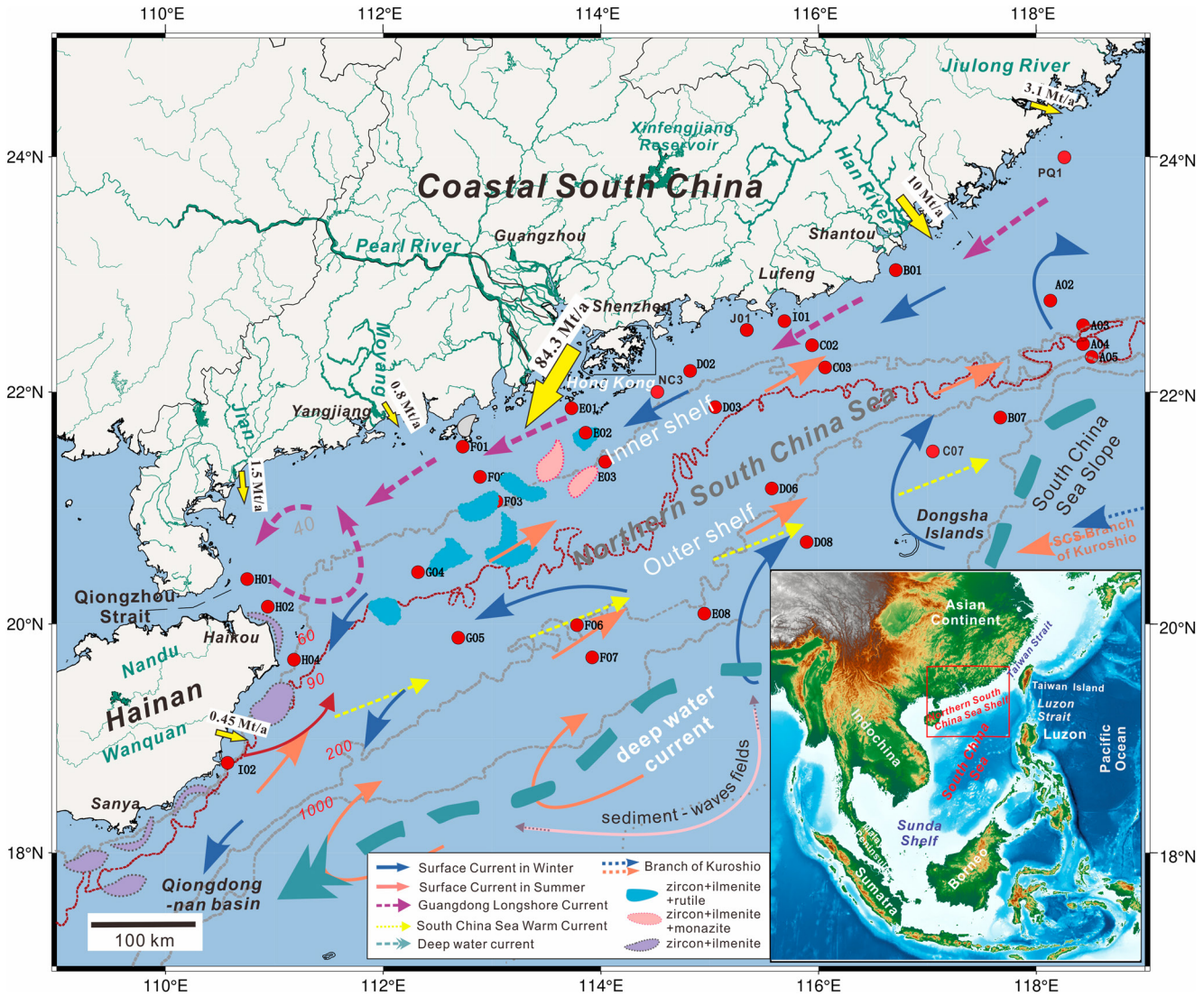

Figure 1. Schematic diagram illustrating the Guangdong Longshore Current and cyclonic eddies to east of the Qiongzhou Strait, surface currents, SCS warm currents, and deep-water currents in the NSCS (refer Fang et al., 2015; Qu et al., 2004; L. Zhong et al., 2017). Red dots note the sampling sites in this voyage. Heavy mineral deposits in the NSCS are also shown (Tan & Sun, 1988; Yang et al., 2005). Inset shows the SCS and its surrounding areas in East Asia.

for reconstructing the last glacial shorelines or the early Holocene coastal regions on Earth. Understanding their temporal-spatial pattern is of particular importance for addressing issues such as changes in the Holocene climate, sea level, and other fields involving the search for placer resources or offshore sands.

The largest and longest zone of relict sediments might be preserved along the outer shelf of the East Asian continental margin from Malaya to Korea across the NSSCS (e.g., Emery, 1968). However, less attention has been paid to the relict sediments despite a significant body of research has been conducted on the sediment supply and Holocene environment during marine resource surveys of the NSSCS over the last five decades (e.g., Cao et al., 2019; Fang et al., 2015; J. Liu et al., 2010; Z. Liu et al., 2010; Tamburini et al., 2003; Tan & Sun, 1988; Wehausen & Brumsack, 2002; Yang et al., 2005; Zhao et al., 2015; L. Zhong et al., 2017; Y. Zhong et al., 2017). The NSSCS is generally subdivided into two hydrographic units of inner and outer shelves across a water depth of −80 m (Figure 1; Jia et al., 2023; Wang et al., 2022; L. Zhong et al., 2017). In the NSSCS inner shelf, the surface sediments were deposited seaward in the order of sand, silt, and clay in response to modern wave dynamics (e.g., Wang et al., 1986). For the surface sediments in the NSSCS outer shelf, two contrasting viewpoints have been proposed (e.g., Cao et al., 2019; L. Zhong et al., 2017; Y. Zhong et al., 2017). One is that the sediments are the relict materials, which have not yet been transported or eroded currently and are unrelated

to the modern hydrodynamic environment (e.g., Cao et al., 2019; Li et al., 1991; Wang et al., 1986). However, the geological, geochemical, and related geochronological evidence for the "relict sediments" has been poorly documented so far. It has also been challenged for the view that "relict sediments" are extensively exposed on the NSSCS sea-floor, as suggested by Emery (1968) (e.g., Luan et al., 2010; McManus, 1975; Shen et al., 2021; Swift et al., 1971). Others suggested that the surface sediments were reworked in the modern environment and thus might not be categorized as relict sediments (Huh et al., 2011; Jia et al., 2023; Li et al., 1991; Swift et al., 1971; L. Zhong et al., 2017; Y. Zhong et al., 2017). A line of evidence shows that the relict sediments are distinct from the alongshore- and seaward-fining modern sands supplied from the adjacent estuaries, beaches and cliffs (e.g., Emery, 1968; Swift et al., 1971); thus, the surface sediments in the NSSCS outer shelf need to be revisited, which is the focus of this paper. Here we investigate how the relict sediments are distinguished from the modern sediments by (a) a depositional setting that is distinctly different from the present environment, (b) traces of remnant fauna or flora, and (c) the expression of ancient (or end of the Pleistocene) shoreline topography. This paper presents the accelerator mass spectrometry (AMS) ^{14}C dating results for in situ shell, sedimentological, and whole-rock geochemical data of the surface sediments collected from 30 sites in the NSSCS. Based on these new data, along with the reported particle-size data (Cai et al., 2013, 2019; Wang et al., 2022; Xu et al., 2016; L. Zhong et al., 2017; Y. Zhong et al., 2017), we reconstruct the discharge pathway for the modern sediments along the Pearl Estuary Channel, draw the spatial patterns of the modern and relict sediments, and discuss the early Holocene (~10 ka) coastal delta or the last glacial shoreline on the NSCS.

2. General Background and Analytical Methods

2.1. General Background

The South China Sea (SCS) is located at the junction of the Eurasian, Pacific, and Australian plates (Figure 1), and is the largest marginal sea in the western Pacific. It is bounded by the Indochina Peninsula, Coastal South China, the Manila Trench, and Palawan-Borneo to the west, north, east, and south, respectively (Wang & Li, 2009). The SCS covers an area of 3.5×10^6 km^2 and has a maximum water depth of more than 5,000 m (e.g., Li et al., 2016). Diverse marine sediments are delivered to the SCS as suspended sediments and dissolved materials from coastal areas via main rivers (Table S1 in Supporting Information S1 and Figure 1; e.g., Chung et al., 2004; Ding et al., 2019; Zhu et al., 2010). The continental shelf is well-developed in the northern and southern SCS (Li et al., 2016).

The NSSCS, with a relatively flat shelf and a width of more than 1,600 km, extends to the south into the slope-shelf transform zone at the −200 m isobaths (Figure 1), at which the sea-floor topography is very complex, with extensive development of submarine terraces, deltas, shoals, underwater valleys, sand dunes, and mass-transport deposits (e.g., Yim et al., 2006). This region is also dissected by numerous submarine canyons and slope gullies that channel the sediments from the shelf of the SCS to the deep-sea region (Figure 1; e.g., Chiu & Liu, 2008; Gong et al., 2015; Li et al., 2016). Over the NSSCS, the oceanic circulation is heavily impacted by the surface current, the Guangdong Longshore Current, the SCS warm current, upwelling currents, KI, and northwestward flow of deepwater from the western Pacific through the Luzon Strait (Figure 1; e.g., Fang et al., 2015; Hu et al., 2000; Liu et al., 2016; Qu et al., 2004). In the NSSCS inner shelf, hydrologic characteristics induce the development of low salinity and high-suspended sediment contents due to the input of terrestrial materials (e.g., Pan et al., 2015).

The NSSCS outer shelf is dominated by high salinity and low suspended-sediment contents due to the involvement of open oligotrophic materials (e.g., Pan et al., 2015; Su & Pohlmann, 2009; Xu et al., 2016). Currents are driven by the East Asian monsoon winds, and the NSSCS surface circulation is characterized by cyclones (counterclockwise) in winter and anticyclones (clockwise) in summer, respectively (Fang et al., 1998; Shaw & Chao, 1994; Su, 2004). The Guangdong Longshore Current is also bimodal, flowing southwestward in winter and northeasterly in summer. However, since the monsoon wind in winter is presently stronger than that in summer (Chu & Guihua, 2003), the net flow of the Guangdong Longshore Current is running toward the southwest. To the east, the Kuroshio Intrusion (KI) enters the northern SCS (NSCS) across the Luzon Strait, a deep-water exchange channel linking the SCS with the western Pacific Ocean (e.g., Li & Gong, 2016; Wang & Li, 2009). The KI induces the southwestward movement of the seawater and transport of suspended sediments along the northern slope of the SCS (Fang et al., 2015; Liu et al., 2016; Webster & Peter, 1994). In addition, mesoscale anticyclonic eddies have been observed along the continental slope from SW Taiwan to the Dongsha Islands, reflecting the detachment of warm loops from the KI (Figure 1; Caruso et al., 2006; Hu et al., 2000; Yuan et al., 2006).

A large number of terrestrial material flows into the NSCS annually, with discharge amounts of up to ~64 and ~13 Mt/yr from SW Taiwan and the Luzon Arcs, and ~84.3, ~10, 0.8, and ~0.45 Mt/a via the Pearl, Han, Moyang, and Wanquan estuaries, respectively (Figure 1 and Table S1 in Supporting Information S1; Liu et al., 2016; Milliman and Farnsworth, 2011; Yim et al., 2006; Zhang et al., 2012). However, the sediments discharged from the Pearl River Estuary are largely deposited on the SW inner shelf with low mass accumulation rates, whereas those from SW Taiwan mainly flow to the NE continental shelf of the NSCS (e.g., Ge et al., 2014; Hu et al., 2014; Liu et al., 2012). In contrast, the transport volumes are low for the sediments from Luzon to the NSSCS due to the KI influence (J. Liu et al., 2008; Z. Liu et al., 2008; Liu et al., 2011). The surface sediments of the NSSCS inner shelf are dominated by high suspended-sediment concentrations due to the terrestrial input from rivers in Coastal South China (e.g., Pan et al., 2015). They are normally reported as terrigenous muddy sediments with the mineral assemblage dominated by ilmenite, zircon, chlorites and sericite (e.g., Liu et al., 2012). However, the surface sediments on the NSSCS outer shelf are dominated by high salinity and little-suspended sandy sediments (e.g., Liu et al., 2012; Pan et al., 2015; Su & Pohlmann, 2009; Xu et al., 2016).

2.2. Sample Collection and Methodology

The 30 surface sediments were collected from the NSCS via the 2016 and 2021 marine voyages of Sun Yat-sen University (China) using the Guangzhou Marine Geological Survey No. 10 and 16 Survey Vessel, and the scientific drilling at the Pearl River Estuary. The sampling sites are shown in Figure 1. The grab apparatus are Van Veen Grab Samplers, and the sampling methods follow Cai et al. (2013) and Xu et al. (2016). The collected surface sediments, with the thickness of 5 cm, were sealed in clean polyethene zipper bags, refrigerated at 4–6°C, packaged, and transported. The vacuum freeze-dried 150 mg sediment samples were pretreated for particle-size analysis.

The in situ shells from the surface sediments were selected for radiocarbon ^{14}C isotopic dating via accelerator mass spectrometry (AMS) to approximate the deposition time and discriminate relict sediments from modern sediments. The surface contaminants on the shells were removed using dilute hydrochloric acid, and the shells were dissolved in phosphoric acid to produce CO_2 for analysis. The pretreatment and ^{14}C measurements were conducted at Beta Laboratories, USA, and the in situ shell ^{14}C dating data were calibrated using the CALIB 8.1 software from the MARINE20 database (Heaton et al., 2020; Stuiver et al., 1998). The calibrated ages are reported as before CE 1950 (cal yr B.P.).

The pre-treatment process of grain size analysis of all 30 samples removed carbonate and organics as they were alternatively soaked in 10 ml of 10% H_2O_2 and 10 ml of 10% HCl solution in clean 50 ml centrifuge tubes for one day to chemically remove the organic matter and calcium carbonate (e.g., Switzer & Pile, 2015). They were washed with deionized water till neutral pH, after which, 5 ml of 5% hexametaphosphate solution was added to deflocculate the samples before sediment particle size was measured after ultrasonic oscillation for 3 min using the Malvern 3000 laser particle analyzer at the Guangdong Provincial Key Laboratory of Geodynamics and Geohazards (GPKLGG), Sun Yat-sen University (China). The measurement repeatability error was less than 1% (Blott & Pye, 2001).

For geochemical analyses, ~5 g sub-samples were crushed in a steel mortar and powdered in an agate mill to a grain size of 180–200 mesh (~75–80 μm). The ~0.5 g sample powders are selected for major oxides analyses using the ARL-Perform X4200 X-ray fluorescence spectrometer at GPKLGG, with relative standard derivations for major oxides being generally maintained within 5%. About 50 mg powders for trace elemental analyses were mixed with 3.6 g $Li_2B_4O_7$, 0.4 g LiF, 0.3 g NH_4NO_3 and minor LiBr in a platinum pot and melted in a glass disc using a high-frequency melting instrument. Trace elemental measurement was performed using an inductively coupled plasma mass spectrometer at GPKLGG, with analytical precision of <5% for >10 ppm elements, 8% for <10 ppm elements, and ~10% for transition metals, respectively.

3. Analytical Results

3.1. In Situ Shell AMS ^{14}C Dating Results

The shells of benthic organisms are commonly used as materials for dating the maximum deposition age of sediments (e.g., Ishizawa et al., 2020). Our new AMS ^{14}C dating results for the 21 undamaged shells from the

NSCS are presented in Table 1 and Figure 2. In situ shells from the surface sediments collected at sites A02, B07, C07, E08 and F06 yield the calibrated age-span in 95.4% probability of 41,507–40,535, 45,333–43,152, 35,129–34,270, 22,599–22,082 and 42,207–41,260 cal B.P., with the median ages of 40,942, 44,312, 34,655, 22,336 and 41,780 cal B.P., respectively. The shells from the surface sediments at sites D06, D08, F07, G05 and PQ1 give AMS ^{14}C calibrated median ages of 9,531 (9,734–9,374), 10,314 (10,507–10,146), 19,235 (19,493–18,966), 12,260 (12,482–1,1991) and 10,492 (10,690–10,270) cal B.P., respectively. In contrast, the in situ shells from the surface sediments at sites A04, B01, C03, D03, E03, F02, G04, and NC3 have relatively young AMS ^{14}C calibrated median ages of less than 1.0 ka cal B.P (Table 1). The shells for the I01 and J01 surface sediments gave AMS ^{14}C calibrated age ranges of 4,148–3,741 and 1,689–1,349 cal B.P. with median ages of 3,949 and 1,512 cal B.P., respectively. Such dating results indicate that the shell AMS ^{14}C calibrated median ages are predominantly young (≤4 ka) and old (≥10 ka), for the surface sediments with water depths of 0 to −80 m and −100 to −400 m in the NSCS, respectively, as shown in Figure 2.

3.2. Particle Size of Surface Sediments

The NSCS surface sediments show considerable variability in composition, with the range of 0%–97% sand (average ∼26%), 1%–78% silt (average ∼52%), and 0%–54% clay (average ∼21%). On the NSSCS inner shelf, the surface sediments show a clear seaward fining trend, at which sand content drops off whereas silt and clay content increases with increasing water depth. In contrast, the surface sediments on the outer shelf are largely composed of well-sorted, medium- and coarse-grained sands (Table S2 in Supporting Information S1). Their particle size, a key parameter for probing the hydrodynamic conditions, is jointly controlled by factors such as sediment provenance, topography, and hydrodynamic conditions. Our new data, together with the reported data from Cai et al. (2013), Xu et al. (2016), L. Zhong et al. (2017), Y. Zhong et al. (2017), and Wang et al. (2022), reveal that the particle size ranges from 0.31 to 8.29φ (φ = $-\log_2$D with D = diameter in mm), with an average value of 5.15φ, in the NSCS (Figures 3a and 4, Tables S2 and S3 in Supporting Information S1).

For those surface sediments on the NSCS slope with a water depth exceeding 500 m, the particle sizes were dominated by silt and clay sediments with Mz values ranging from 4.78 to 8.29φ (n = 70, peaks at 7.4 and 8.1φ; inset Figure 3a). However, the surface sediments with a water depth of 0 to −400 m on the NSCS have variable particle sizes from 0.31 to 8.20φ (n = 272), with a main peak at 5.3φ and four secondary peaks of 1.3, 2.5, 4.3 and 6.1φ (inset in Figure 3a). The skewness, kurtosis, and sorting coefficient are −0.80–0.35, 0.62–8.40, and 0.38–3.95 (averages of −0.19, 1.16, and 2.09), respectively.

The surface sediments on the continental slope are generally fine (Figures 3a and 4). The coarse-grained sediments predominately occur along the Qiongzhou Strait and the Pearl River and Han River estuaries. In the northeastern domain, the surface sediments are coarser than those in the southwestern domain of the NSCS. In addition, a pattern of fine–coarse–fine–coarse–fine sediments could be observed from the NSCS north (near-shore) to south (slope). Such a spatial pattern suggests that sediment transport is controlled by a combination of underwater geomorphology, hydrodynamic conditions, and sediment exchange via traction, scouring, and suspension mechanisms (e.g., Luo et al., 2013). Notably, four domains with relatively coarse-grained sands could be distinguished in this dataset, including the Pearl Estuary Channel (Area I), NW Shenhu (Area II), NW Dongsha (Area III) and Taiwan Shoal (Area IV).

The surface sediments in the Pearl Estuary Channel (Area I) are composed of medium-to coarse sands and clay, exhibiting a bimodal pattern (Figures 3b and 4). In Taiwan Shoal (Area IV), the sediments are unimodal and consist of well-sorted, medium- and coarse-grained sands, as shown in Figure 3b. In contrast, polymodal and mixed sediments are identified on the NSCS modern shoreline and outer shelf (Area II and III; Figure 3c), potentially suggesting a multi-provenance supply or complex hydrodynamic conditions in the regions.

3.3. Geochemical Records

The geochemical characteristics of the NSCS surface sediments might provide key constraints for the depositional environment and source-to-sink process (e.g., Cullers, 2000). As presented in Table S4 in Supporting Information S1 and Figures 5a and 5b, the surface sediments have a chemical index of alteration (CIA) ranging from 10.5 to 90.4 with an average value of 47.8. Al/Na = 3.53–134 (averages of 10.72), K/Al = 0.08–0.78 (averages of 0.23), MnO/TiO_2 = 0.04–1.41 (averages of 0.12) and Cr/Al_2O_3 = 1.07–23.3 (averages of 2.59), respectively.

Journal of Geophysical Research: Earth Surface

10.1029/2023JF007125

Table 1
In Situ Shell AMS ^{14}C Dating Results From the Surface Sediments at the Sites in the Northern South China Sea

Sample number	Longitude (East)	Latitude (North)	Dating material	Measured age (B.P.: Before present)	Calibrated age-span probability (cal B.P.)[a]	Calibrated median age (cal B.P.)[a]	IRMS $\delta^{13}C$ (‰)	IRMS $\delta^{18}O$ (‰)	Beta lab number
Relict sediment from the outer zone of northern shelf of the South China Sea									
A02-surface	118.1257	22.7841	Shell: acid etch	36,880 ± 350	41,507–40,535, 95.4%	40,942	+2.2	−1.22	625718
B07-surface	117.6719	21.7778	Shell: acid etch	42,230 ± 640	45,333–43,152, 95.4%	44,312	−0.3	−0.94	638304
C07-surface	116.7131	21.3270	Shell: acid etch	30,900 ± 190	35,129–34,270, 95.4%	34,655	+1.8	+1.49	625717
D06-surface	115.5676	21.1657	Shell: acid etch	8,870 ± 30	9,734–9,374, 95.4%	9,531	+1.5	+0.08	625726
D08-surface	115.8923	20.7097	Shell: acid etch	9,450 ± 30	10,507–10,146, 95.4%	10,314	+2.0	+1.47	615091
E08-surface	114.9495	20.0867	Shell: acid etch	19,110 ± 60	22,599–22,082, 95.4%	22,336	+3.9	+1.14	632795
F06-surface	113.7803	19.9895	Shell: acid etch	38,180 ± 400	42,207–41,260, 95.4%	41,780	+2.6	+0.89	632784
F07 (12 cm)	113.9247	19.7055	Shell: acid etch	16,540 ± 50	19,493–18,966, 95.4%	19,235	+0.5	+2.70	632788
G05-surface	112.6855	19.8815	Shell: acid etch	10,790 ± 30	12,482–11,991, 95.4%	12,260	+0.3	+0.66	625715
Modern sediment from the inner zone of northern shelf of the South China Sea									
A04-surface	118.4252	22.4109	Shell: acid etch	12,40 ± 30	924–638, 95.4%	776	+0.4	−0.41	632799
B01 (50 cm)	116.7052	23.0407	Shell: acid etch	790 ± 30	526–252, 95.4%	392	+0.3	−0.50	537533
C03-surface	116.0594	22.2132	Shell: acid etch	105.11 ± 0.39 pMC		Present		+0.06	638300
D02 (29 cm)	114.6848	22.3589	Shell: acid etch	350 ± 30	158–present, 94.8%	Present	−0.5	−1.38	614708
D03-surface	115.0451	21.8720	Shell: acid etch	109.92 ± 0.41 pMC		Present	+0.1	−0.32	625733
E03-surface	114.0361	21.4000	Shell: acid etch	103.42 ± 0.39 pMC		Present	−0.2	−0.39	638299
F02-surface	112.8864	21.2665	Shell: acid etch	530 ± 30	283–present	139	+1.1	−0.50	638303
G04-surface	112.3174	20.4479	Shell: acid etch	450 ± 30		Present	+1.8	−1.85	632798
I01-surface	115.7134	22.6797	Shell: acid etch	3,940 ± 30	4,148–3,741, 95.4%	3,949	+1.5	−0.21	610690
J01 (17 cm)	115.2438	22.5445	Shell: acid etch	1,960 ± 30	1,689–1,349, 95.4%	1,512	+1.8	−0.46	610694
NC3 (35 cm)	114.5383	22.0516	Shell: acid etch	1,330 ± 30	1,025–699, 95.4%	859	+0.9	−1.05	610897
PQ1-surface	118.2240	23.9300	Shell: acid etch	9,590 ± 30	10,690–10,270, 95.4%	10,492	+1.2	−2.78	615086

[a]Notes the calibrated in situ shell. ^{14}C age results using the CALIB 8.1 software from the MARINE20 database (Heaton et al., 2020; Stuiver et al., 1998). cal yr B.P. notes before CE 1950.

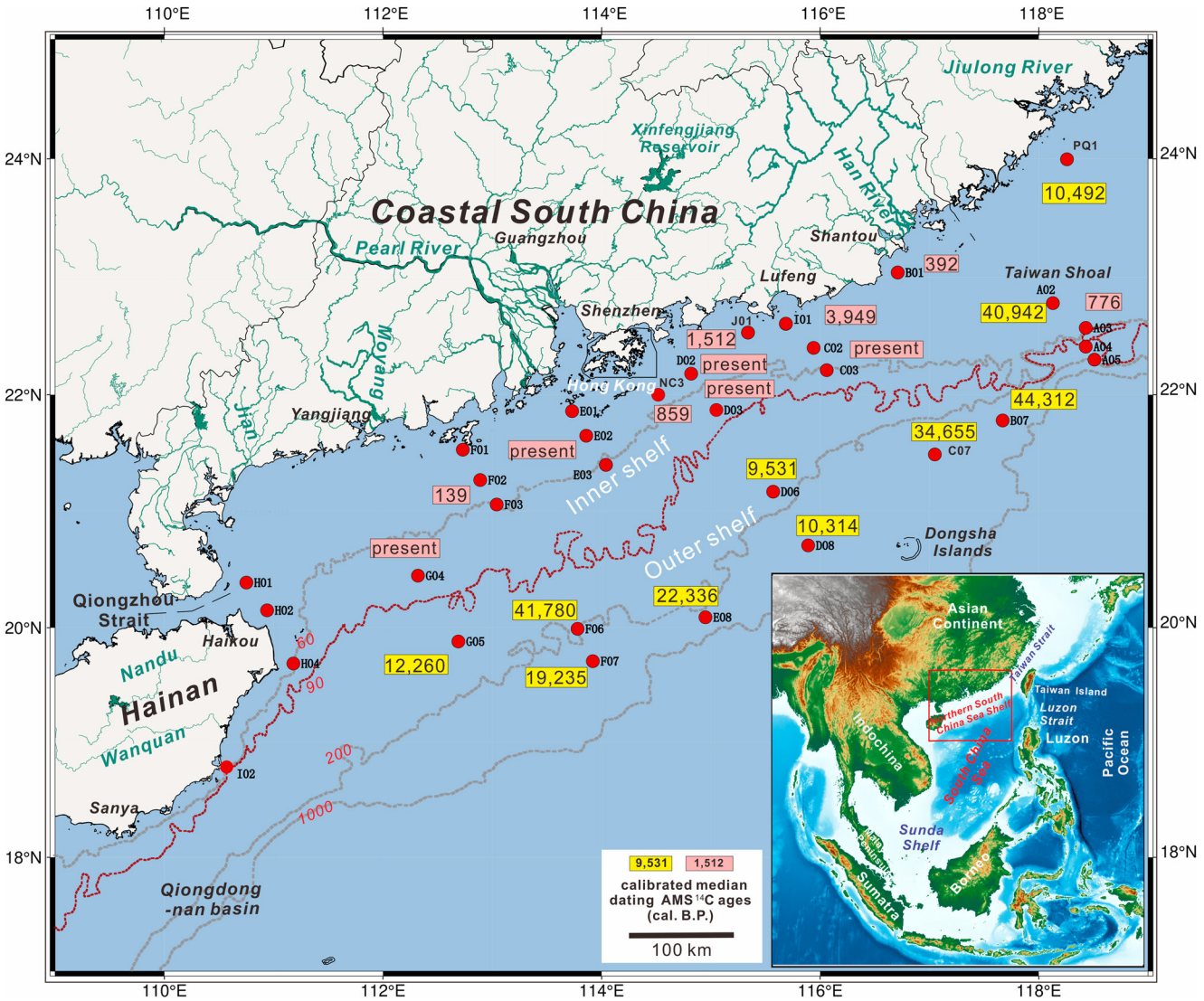

Figure 2. Spatial patterns of in situ shell AMS ^{14}C calibrated median ages for the NSCS surface sediments collected during this voyage. Numbers with pink and yellow squares note the relatively older and younger AMS ^{14}C median ages (cal B.P.) for in situ shells from the surface sediments, respectively. Dashed lines with numbers denote the isobaths.

Their Zr/Sc ratios are in the range of 6.58–56.9 with averages of 15.5. The geochemical indicators define the beaded pattern in Figures 5a–5c. The surface sediments in the NSSCS inner shelf generally have higher CIA and Al/Na values than those in the outer shelf. Conversely, K/Al ratios are higher while Al/Na and CIA are lower for the surface sediments along the outer shelf and at the Taiwan Shoal, in contrast to those in the modern Guangdong offshore (Figures 5a–5c).

A large number of terrestrial materials is transported via rivers and channels into the NSCS continental shelf and then deposited under suitable hydrodynamic conditions (e.g., Zhang et al., 2012; Zong et al., 2012). Such a process is highly influenced by sea-level change and sediment supply. Particular elements can be used as effective source indicators because they or their ratios are transferred quantitatively into sediments from terrestrial parent rocks during weathering, erosion and transport, which would not usually be affected by diagenesis (McLennan et al., 1990). Rare earth elements (REEs) and their ratios mostly exhibit similar behaviors when entering the environment, and thus are commonly used as geochemical indicators in clastic systems (e.g., Su & Pohlmann, 2009). Major element aluminum (Al) is commonly well conserved in clastic sediments (Fralick & Kronberg, 1997), also immobile trace elements, for example, cobalt (Co), chromium (Cr), nickel (Ni), rubidium (Rb), scandium (Sc), vanadium (V), and zirconium (Zr) (McLennan et al., 1990). Scandium and Cr mainly from terrigenous

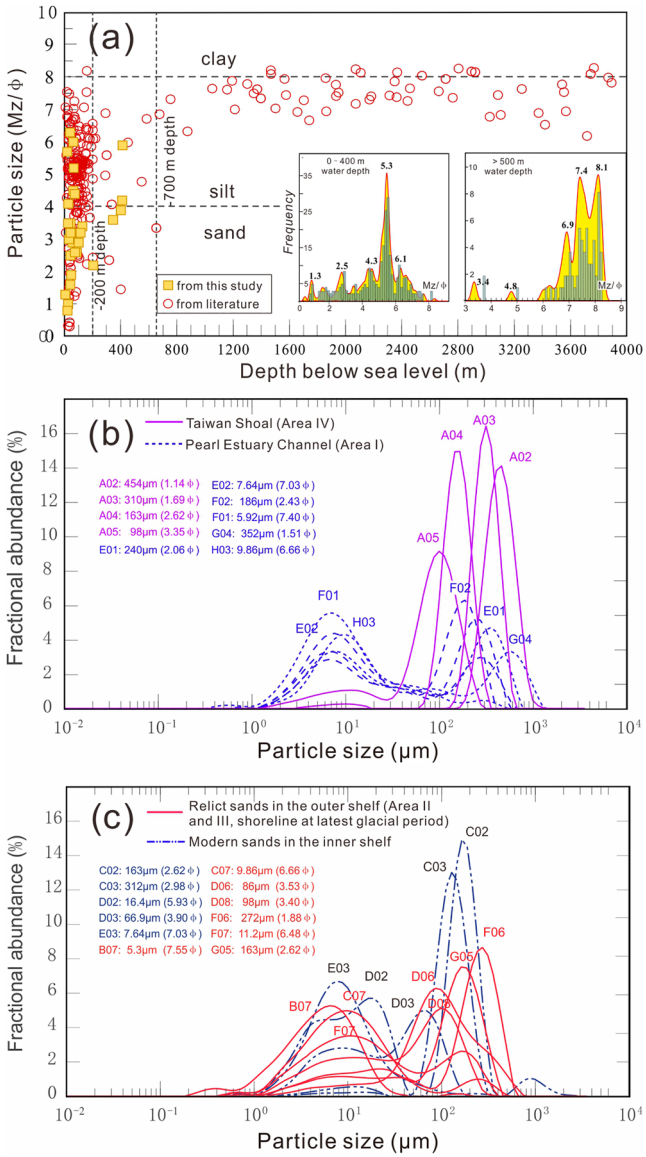

Figure 3. (a) Variation of particle sizes (Mz/φ) with the increasing water depth for the NSCS surface sediments. Insets show the frequency of particle sizes for the surface sediments with the water depths of 0–400 m and >500 m, respectively. Data with circles are from Cai et al. (2013), Xu et al. (2016), L. Zhong et al. (2017), Y. Zhong et al. (2017) and Wang et al. (2022), and others with yellow squares are from this study. (b, c) Frequency of the particle sizes (μm) for the NSCS surface sediments in Area I, II, III and IV in Figure 6. Data in (b, c) are from this study.

provenance travel further through the source-to-sink pathway. However, Zr and Ti are preferentially preserved in the surface sediments via river transportation due to their enrichment in heavy minerals and their resistance to chemical weathering. To minimize the impacts of particle size on the immobile element contents of the surface sediments (Wang et al., 2022), Cr/Al_2O_3 and Zr/Sc ratios could be proxies for the seaward discharge and short-distant transportation in response to high-energy hydrodynamics (e.g., Bhatia & Taylor, 1981; Carlson et al., 2008; Wronkiewicz & Condie, 1987).

Our dataset shows that the surface sediments have high Cr/Al_2O_3 ratios in the Han and Pearl estuaries, the Taiwan Shoal, the NW Shenhu and NW Dongsha on the outer shelf (Figure 5d). Notably, spotted enrichment could be observed in the NW Shenhu and NW Dongsha areas (Figure 5). Similar enrichment is also shown in the MnO/TiO_2 contour map (Figure 5f). On the NSCS inner shelf, enrichment in Zr/Sc is given in not only the Han Estuary but also in the Pearl Estuary Channel (Area I). Two small areas with relative enrichment in Zr/Sc are mapped in the NW Shenhu and NW Dongsha. Such signatures collectively suggest that the discharge environment for the surface sediments on the NSCS inner shelf was distinct from that on the outer.

4. Discussion

The modern continental shelves were mostly exposed during the LGM, thus relict sediments should distribute widely on worldwide continental shelves. However, they might be re-activated as the "mixture or palimpsest" sediments due to rapidly- rising sea-level and hydrodynamic condition changes during the post-glacial period, resulting in the relict sediments being only partly preserved in the accommodation space on the continental shelves in some regions (e.g., Chappell & Polach, 1991; Shen et al., 2021; Swift et al., 1971). Flat and broad NSSCS, serving as the perfect region for bearing relict sediments, is dissected by numerous submarine canyons that channel the sediments from the shelf to the deep-sea parts of the system (Figure 1).

The sandy and silty sediments occur widely on the NSCS inner and outer shelves, as well as the upper part of the continental slope, with clay only dominantly preserved on the lower part of the continental slope (Figure 3a). Terrigenous sediments are believed to be transported to the NSSCS continental shelf via local currents that sweep sediments from the Coastal South China river-system to the west. Previous studies showed that the sediments transported by the Red River to the west are mainly discharged into the Beibuwan, Yinggehai, and Qiongdongnan basins due to the obstruction of Hainan Island (e.g., Cai et al., 2013; Li et al., 2012). The sediments from SW Taiwan (~64 Mt/a) are mostly accumulated on the northeastern shelf via the Jhuoshuei Estuary, with only a small amount deposited on the continental slope via the Penghu and Fomosa canyons (Figure 6; e.g., J. Liu et al., 2008; Z. Liu et al., 2008; Liu & Stattegger, 2014). Philippine sources are dominated by the suspension fractions from Luzon Arc (~13 Mt/a), and largely deposited to the northwest of Luzon.

Sedimentation on the NSSCS is driven in part by the surface current, including the Guangdong Longshore Current, a bimodal system driven by the East Asian monsoon winds (Chu & Guihua, 2003). The sediments on the eastern NSSCS are additionally affected by the KI that drives the southwestward movement of seawater and the transport of the suspended sediments along the northern slope of the SCS (Fang et al., 2015; Liu et al., 2016; Webster & Peter, 1994). Thus, the spatial heterogeneity for the NSCS sediments is likely the collective result of different sedimentary provenances, transportation, discharge and hydrodynamic processes (Jia et al., 2023). Their deposited nature and spatial pattern varied significantly from the latest Pleistocene to the early Holocene. Sea-level

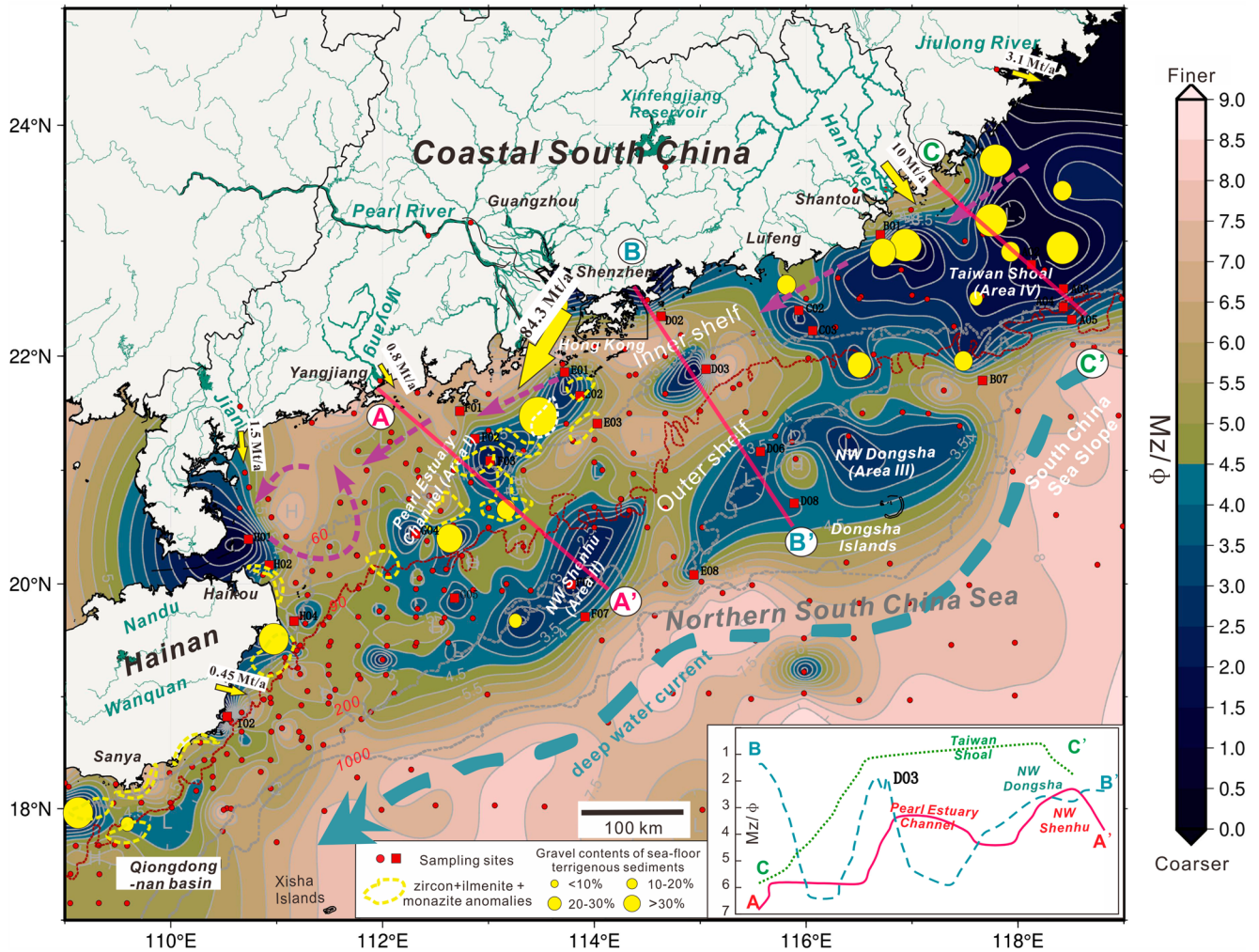

Figure 4. Contour map for the particle size of the NSCS surface sediments. Also shown for the sea-floor gravel-bearing sediments, the heavy mineral deposits, the Guangdong Longshore Current and the deep-water current (Fang et al., 2015; Qu et al., 2004; L. Zhong et al., 2017). The size of the yellow dots notes gravel contents for sea-floor terrigenous sediments (L. Zhong et al., 2017). Areas with yellow dashed lines denote the locations of heavy mineral deposits with elevated zircon, ilmenite, and monazite contents. Sampling sites with dark-red dots are from Cai et al. (2013), Xu et al. (2016), L. Zhong et al. (2017) and Cao et al. (2019) and those with red squares are from this study. The inset also shows the seaward variation for particle size along the A-A', B-B' and C-C' profiles in Figure 4.

change might additionally be a dominant factor as sea level rose from around −90 m around 12–14 ka cal B.P. to a maximum of around 2 m at ~7 ka cal B.P (e.g., Lambeck et al., 2014; Xiong et al., 2018; Zong et al., 2012). Across this time, changes in the shoreline and seafloor topography certainly shaped the distinct deposition environment and spatial distribution of the NSCS sediments (e.g., McManus, 1975). The spatial patterns of the relict, modern and mixture sediments are the key basis for approximating the NSSCS shoreline or coastal delta position during the LGM and assessing Holocene climate and sea-level changes, and sediment source-to-sink processes.

4.1. Identification of Relict Sediments in the Present Outer Shelf

On the basis of the above-mentioned particle size, shell AMS ^{14}C median age, and geochemical data, three distinct surface sediment patterns were identified on the outer shelf, as shown in Figure 6. In particular, we identified two regions of heterogeneous sandy sediments separated by the tail of the Baiyun slide (see Figure 6). One sandy area is situated in the NW Shenhu area (Area II in Figure 6). The other, designated as Area III in Figure 6, is located to the northwest of the Dongsha Islands. The NW Dongsha and NW Shenhu accumulation areas are located at the junction of the westward North Pacific deep-water current branch, the KI, and the SCS warm current (Figures 1 and 6; e.g., Fang et al., 1998; Liu et al., 2012, 2014). Available data show that the North Pacific deep-water branch is unlikely to carry the sediments from SW Taiwan onto the outer shelf across the

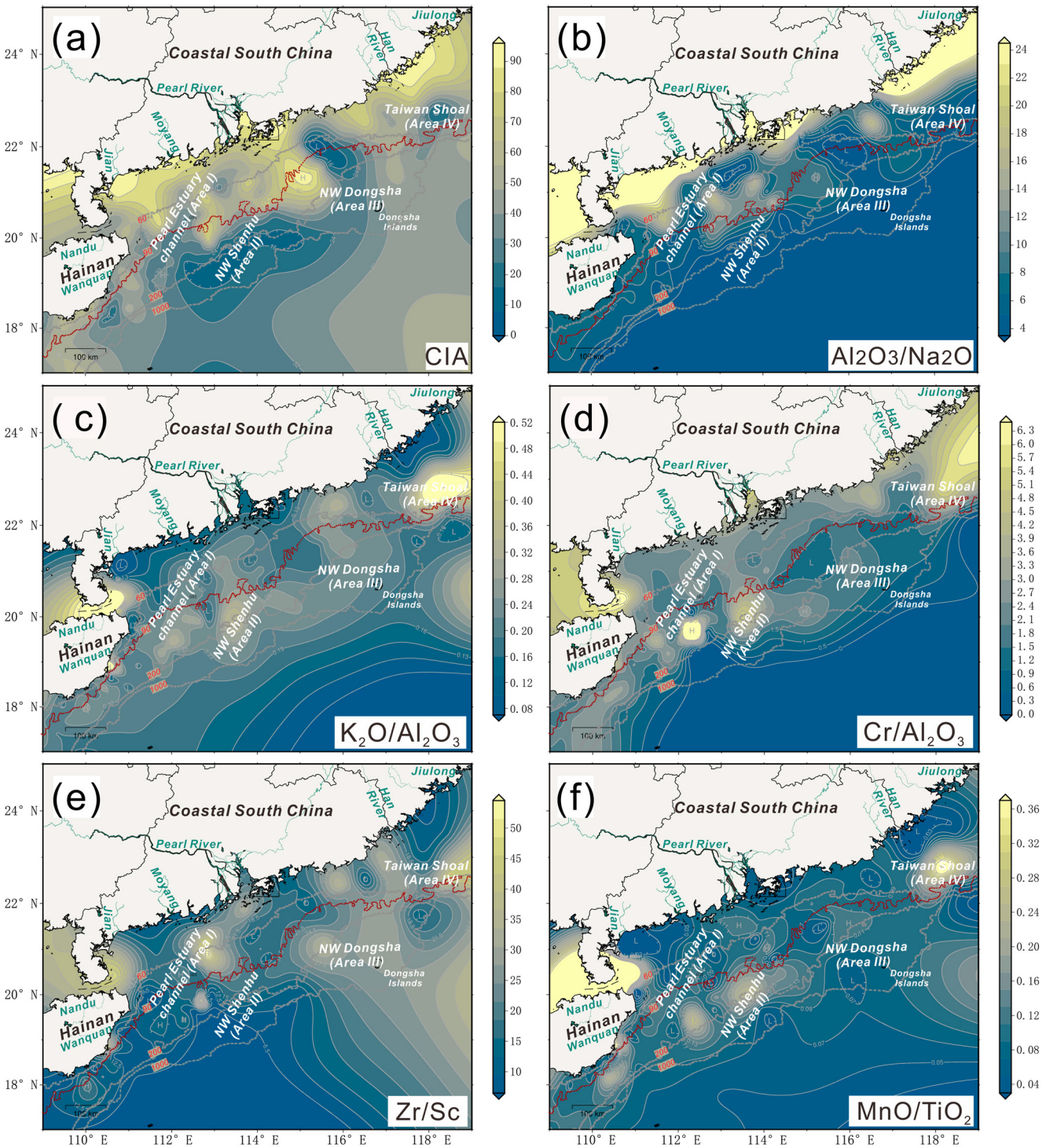

Figure 5. Contour maps of the geochemical indicators for the NSCS surface sediments. Data are from Table S4 in Supporting Information S1. (a) CIA (Al_2O_3/(Al_2O_3+CaO*+Na_2O + K_2O)*100), (b) Al_2O_3/Na_2O, (c) K_2O/Al_2O_3, (d) Cr/Al_2O_3, (e) Zr/Sc and (f) MnO/TiO_2, respectively.

NSCS continental slope (e.g., Shao et al., 2007; Wang, 1999). In response to the KI, the sediments from SW Taiwan and Luzon are commonly transported to the southwest of the Dongsha Islands, and then into the Xisha Trough along the NSCS continental slope (e.g., Chen et al., 2014; Li & Clift, 2013). Sediments from Luzon are poorly discharged onto the NSCS outer shelf, as revealed by the magnetic susceptibility pattern of the surface sediments (Figure 6; Liu et al., 2009, 2011; Y. Zhong et al., 2017). In addition, the sediment supply (~13 Mt/a)

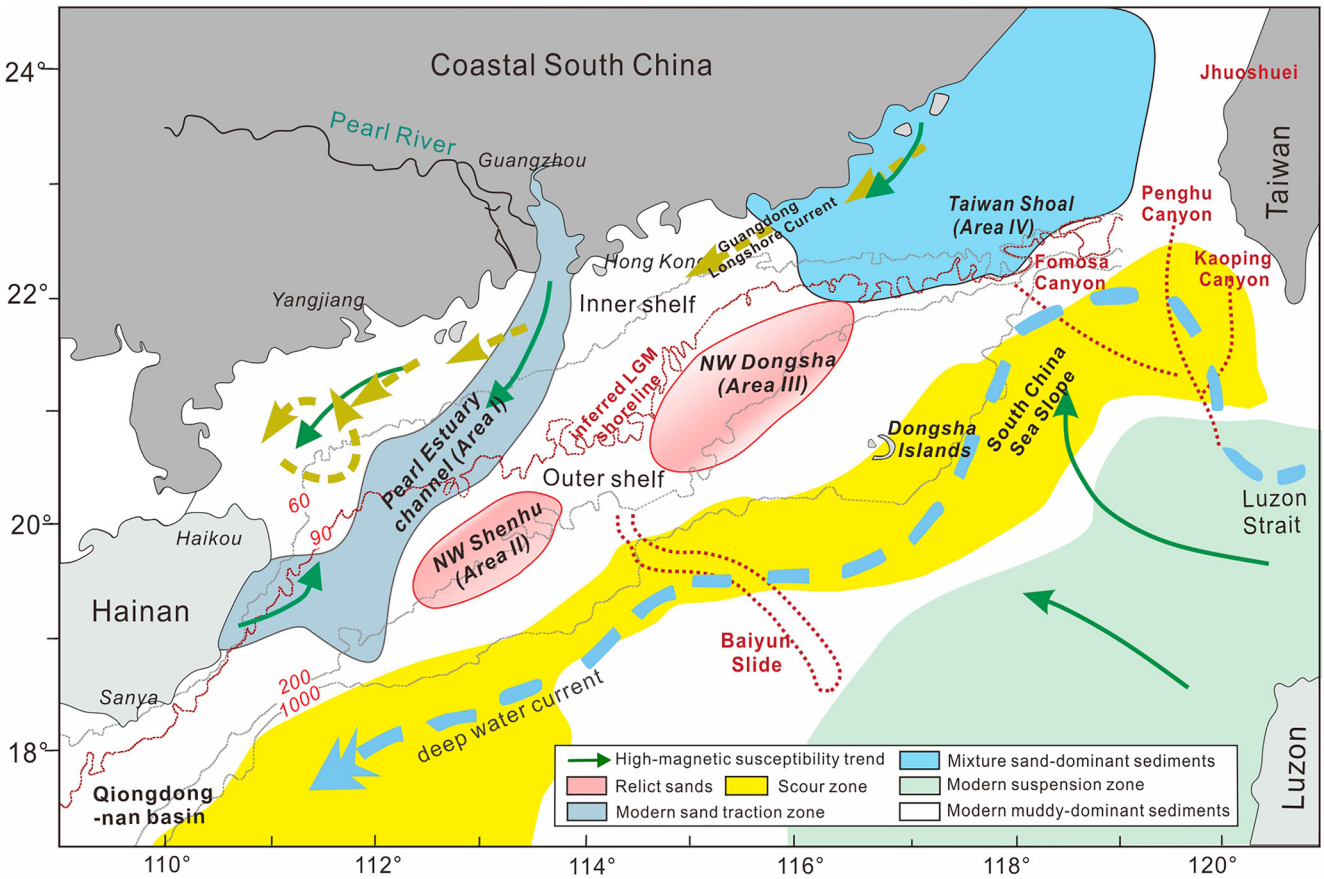

Figure 6. Spatial patterns for the modern, mixed and relict sediments on the NSCS. The inferred last glacial shoreline is also shown. Green marks noting the high-magnetic susceptibility trend are from Liu et al. (2009, 2011) and Y. Zhong et al. (2017).

from Luzon is characterized by high-suspended fractions with little bed-load transport. Naturally, the coarser sand dunes in the NW Dongsha area (Area III) are unlikely supplied by the KI (Reeder et al., 2011), and are thus proposed herein to be of relict origin.

Available data show that the depositional rate remained relatively low for the surface sediments in the NSCS inner shelf since the Holocene (e.g., Cao et al., 2019; Fang et al., 1998; Ge et al., 2014). With such a low depositional rate, the near-shore coarse-grained or fluvial sediments are difficultly transported in large quantities onto the NSCS outer shelf via the Guangdong Longshore Current (e.g., Cao et al., 2019; Ge et al., 2014). In fact, the Guangdong Longshore Current may have limited influence on sedimentation on the outer shelf. One explanation is that the suspended sediments on the NW inner shelf were reworked into the NW Shenhu area by strong wave-induced currents. However, the reworked sediments are usually fine-grained or clay under such conditions, contradicting our observation that the surface sediments in the NW Shenhu are dominated by the coarse-grained sands (Figure 4). Therefore, the alternative is that the eastward SCS warm current on the outer shelf is responsible for the transport and discharge of the coarse-sandy sediments in the NW Shenhu and NW Dongsha. However, the SCS warm current has an average current velocity of ~0.25 m/s (Wang et al., 2011), far lower than the minimum velocity of ~0.55 m/s for carrying the sandy sediments (e.g., L. Zhong et al., 2017). That is to say, the large-scale coarse-grained sediments in the NSSCS outer shelf were unlikely to be transported from the Pearl Estuary Channel (Area I) or the offshore area of Eastern Hainan via the SCS warm current (e.g., Li et al., 2008; Lüdmann et al., 2001). Thus, the coarse-grained sands in the NW Dongsha and NW Shenhu of the NSSCS outer shelf are unlikely to be of modern origin (e.g., L. Zhong et al., 2017). Instead, they are either relict sands or mixtures of modern with relict sediments (e.g., Cao et al., 2019; Li et al., 2008; Lüdmann et al., 2001; Y. Zhong et al., 2017).

The hypothesis of the relict origin is supported by in situ shell dating from the surface sediments in the NSCS outer shelf (Table 1 and Figure 2). Their dating results give the AMS ^{14}C median ages ranging from ~10 to ~45

ka cal B.P. This temporally corresponds to the last glacial period of the Late Pleistocene, reflecting the "relict" nature of the sediments. During the LGM, the sea-level of the NSSCS was likely −70 to −130 m below that of today (e.g., Ge et al., 2014; Xiong et al., 2018; Zong, 2004; Zong et al., 2012). As shown in Figures 4 and 6, the sandy sediments in the NW Shenhu and NW Dongsha are generally limited to the sites deeper than (to the south of) the present −90 m isobaths. Such characteristics suggest that the NW Shenhu and NW Dongsha sandy accumulation regions were topographically located near the LGM shoreline (e.g., Emery, 1968).

The geochemical parameters (e.g., CIA, Al/Na, K/Al, Cr/Al_2O_3, Zr/Sc, MnO/TiO_2) and heavy mineral contents (zircon, rutile and ilmenite) are responsive to changes in the depositional environment (e.g., Wang et al., 2020, 2022). CIA is known as a robust indicator for probing climate changes, which sharply increases across the glacial-interglacial transitions, reflective of distinct chemical weathering intensity (e.g., Wang et al., 2020). In general, surface sediments have lower K/Al ratios but higher Al/Na and CIA under hot and humid conditions compared with those in the cold and dry environment, at which low chemical weathering rates result in the preferential leaching of CaO, Na_2O and K_2O during clay mineral formation (e.g., Nesbitt et al., 1980; Singh et al., 2005).

Our geochemical data define the distinct pattern in Al/Na, K/Al, and CIA for the NSCS inner and outer shelves, as shown in Figure 5. The sediments on the Taiwan Shoal and partly along the outer shelf are characterized by higher K/Al but lower Al/Na and CIA values, indicating a stronger physical weathering. Such signatures suggest that the depositional environment on the outer shelf was colder and drier, distinct from the hot and humid modern environment on the NSSCS inner shelf, which is consistent with what would be expected for the relict and modern sediments (e.g., Emery, 1968; Swift et al., 1971). Similar considerations are also suggested by Ti/Na and K/Na contours (not shown). Collectively, these data indicate that the sandy sediments are of the latest Pleistocene (∼12–40 ka) to ∼10 ka early Holocene (i.e., relict) origin in the NW Shenhu and NW Dongsha areas.

4.2. Modern Surface Sediments in the Present NW Inner Shelf

For the NW inner shelf of the NSCS, the sediments are predominantly supplied by the Pearl River system with minor from the Moyang and Wanquan rivers (Figures 1 and 6; Cai et al., 2013; Liu et al., 2012, 2014; L. Zhong et al., 2017). In situ shell AMS ^{14}C median ages for the surface sediments range from <4 ka B.P. to the present time, suggesting that the deposition occurred in the middle to late Holocene. In the central NW inner shelf, a NE-trending zoning channel, referred to as the Pearl Estuary Channel, was mapped from the Pearl River estuaries to the offshore area of NE Hainan (Area I in Figures 4–6). The surface sediments in this channel are characterized by medium- and coarse-grained sands with high Zr/Sc and magnetic susceptibility values (Figures 4–6), suggesting a relatively high-energy environment. Such a channel also overlaps the areas of the reported heavy mineral deposits and gravel-bearing sediments with the indicators of high-energy transport (Figure 4; Tan & Sun, 1988; Zhang et al., 1992). The terrestrial sediments were transported to the NW continental shelf along the pathway channel via fluvial processes.

Two potential mechanisms might be proposed for the sandy supply in Area I (Figures 4 and 6; e.g., Li et al., 2015; L. Zhong et al., 2017). One is from Hainan via the Wanquan and Nandu river estuaries. However, as shown in Figures 1 and 4, the sandy and gravel-bearing sediments, and the heavy minerals transported from Hainan only occur in the offshore areas of eastern Hainan (e.g., Zhang et al., 2013). The other is that the sedimentary supply is from Coastal South China via the main rivers. Available data indicate that the sedimentary supply in the NSCS is mainly from the Pearl fluvial drainage system as it exceeds ∼84 Mt/a, far higher than the sediment supply (0.4–1.5 Mt/a) from the other river systems (e.g., Moyangjiang and Jian estuaries), as shown in Table S1 in Supporting Information S1 (Ge et al., 2014; Liu et al., 2011, 2014). As presented in Figure 6, the offshore estuary delta of Area I Channel spatially overlaps the Pearl River Estuary. Thus, the sediments in the Area I Channel are mainly sourced from the Pearl River fluvial system, and the hydraulic sorting during sediment transportation is responsible for the development of heavy mineral deposits. Alongside the coarser zone in Area I, fine-grained suspended particles discharged from the rivers are carried on the continental shelf by the river plume and coastal currents, at which they are transported away from the estuary (Jia et al., 2023). Due to the rapid decrease in flow velocity across the Area I Channel along with the changes in salinity and other properties of the seawater, the fine-grained sediments are likely deposited at the adjacent areas as the bed load mixes with the flocculated materials (Papista et al., 2011). Our data reveal two areas that are dominated by muddy sediments (Figure 4). One is the square-shaped area to the south of Hong Kong, and the other is the longshore area from the Pearl River

Delta to NE Hainan (Figure 6; Ge et al., 2014; Liu et al., 2014). The transportation and discharge of the muddy sediments might be highly controlled by the Guangdong Longshore Current (Figures 1 and 4; Chen et al., 1986; Dong et al., 2004; Y. Zhong et al., 2017). The <~4 ka B.P. in situ shell AMS ^{14}C median ages (Figure 2), decreasing in Cr/Al_2O_3 with increasing seaward distance and water depth, and low K/Al but high Al/Na and CIA for the surface sediments (Figure 5), collectively suggest that the fluvial sediments transported into the NW inner shelf are of modern origin in the hot and humid environment. Their transport and discharge are primarily controlled by the Guangdong Longshore Current and its secondary cyclonic eddies (Figures 4 and 6; Liu et al., 2014, 2016; L. Zhong et al., 2017).

4.3. Mixed Sediments in the Taiwan Shoal and Its Vicinities

The Taiwan Shoal is located on the northeastern inner shelf to the east of the Lufeng–Dongsha line (Figure 1) and is accumulated by abundant land-derived sediments from Coastal South China and Taiwan Island. Except for the fine-grained sands and clays along the Han Estuary and present shoreline, the surface sediments show extremely high compositional maturity and gravel-bearing sediments occur extensively in the Taiwan Shoal and its vicinities (Figure 4, Shen et al., 2021). They are largely composed of coarse-grained sands and rounded quartz indicative of higher energy conditions (Figure 3b). From the Han Estuary to the Taiwan Shoal, particle size for the surface sediments generally increases (inset in Figure 4). Such signatures contradict what would be expected if the sediment transport was mainly controlled by the Guangdong Longshore Current or from the Han fluvial drainage. In addition, the Zr/Sc ratios for the surface sediments are low in the Han and Jiulong estuaries but high in the Taiwan Shoal (Figure 5e). These data are consistent with the hypothesis that the detrital sediments in the Taiwan Shoal and its vicinities are mainly from SW Taiwan via the Jhuoshuei Estuary rather than Coastal South China via Han and Jiulong estuaries (Table S1 in Supporting Information S1 and Figure 4; e.g., Liu & Stattegger, 2014). This is further supported by the fact that the sediment contribution from the Han Estuary is much lower than that delivered from SW Taiwan via the Jhuoshuei Estuary.

Y. Zhong et al. (2017) and Cao et al. (2019) have proposed that the sandy sediments in the Taiwan Shoal might be of relict origin (e.g., Chen, 1993; Niino & Emery, 1961). However, Yu and Song (2000) and Shen et al. (2021) considered that they formed during glacial and interglacial periods and were then reworked by Holocene wind-driven storm waves, thus being a mixture origin (e.g., Ma & Liu, 1994). Our results show that the sediments have high CIA and Al_2O_3/NaO but low K_2O/Al_2O_3 in the Han and Jiulong estuaries, suggestive of the modern hot and humid environment. K_2O/Al_2O_3 and Cr/Al_2O_3 ratios for the sediments in the northeastern inner shelf are higher than those in the northwestern inner shelf (Figures 5c and 5d), indicating their distinct terrestrial supply. On the other hand, for the sediments in the Taiwan Shoal and its vicinities, CIA and Al_2O_3/NaO are relatively low and K_2O/Al_2O_3 ratios are high, reflecting a cold and dry environment. The dotted enrichment in MnO/TiO_2 for the surface sediments in the Taiwan Shoal and its vicinities, resembling those in the NW Shenhu area, might be related to subaerial exposure. Such signatures appear to suggest an origin of relict sediments (Figures 5a–5c). However, as shown in Figure 1, the Taiwan Shoal and its vicinities are situated in the inner zone with the water depth of less than 90 m. The in situ shell AMS ^{14}C median age ranged from 392 cal B.P. to ~41 ka cal B.P. (e.g., A04, B01, A02 and PQ1) for the surface sediments. These data consistently suggest that the sediments is of Late Pleistocene origin (relict sands), which have been reworked in response to the Holocene transgression, the Pacific low-pressure cyclones and the KI. Modern materials from SW Taiwan (major) and southeastern Coastal South China (minor) were heterogeneously added to the relict sediments, developing the mixed sediments in the Taiwan Shoal and its surroundings.

4.4. Reconstruction of the Last Glacial Shoreline or Early Holocene Coastal Delta

Gravel-bearing sediments and heavy mineral deposits can serve as useful indicators for mapping the drainage systems, the coastal delta or the shoreline (e.g., Schlee, 1968; L. Zhong et al., 2017). Figure 1 shows the gravel-bearing sandy sediments and heavy mineral deposits (zircon + ilmenite ± rutile/monazite) on the NSSCS. Such a spatial distribution provides important constraints for shorelines, river channels or coastal deltas (e.g., Li et al., 2015). The surface sediments in the current outer shelf show higher Zr/Sc and Cr/Al_2O_3 than those in the inner shelf, and higher heavy minerals relative to their background values (e.g., Cao et al., 2019; Gao et al., 2008; Wang et al., 2022), suggesting the traction transportation over a short distance. In addition, the MnO/TiO_2 ratios for the surface sediments in the outer shelf are higher than those in the inner shelf, reflecting the subaerial exposure since the relict sands are stained by Fe-Mn oxides (e.g., Emery, 1968).

As mentioned above, the partial sizes for the surface sediments on the NSCS outer shelf exhibit poly-modal patterns, resembling those in the modern Guangdong offshore (Figure 3c). Such signatures, along with the "ancient" in situ shell AMS ^{14}C median ages of ∼10–45 ka cal B.P (Table 1 and Figure 2), indicate that the coarse-grained sands on the current outer shelf might have been deposited in the littoral area during the LGM to the earliest Holocene. This is further supported by the accessory mineral assemblage (zircon-ilmenite-epidote) and gravels of the sea-floor sediments on the outer shelf (Figure 4; e.g., Liu et al., 2012). Thus, our data suggest that the ancient Pearl River Estuary should be undercut across the present inner shelf in response to the lowering sea-level at the last glacial period (e.g., Yang et al., 2008). Abundant sandy sediments flowed southward from the exposed inner shelf via the "ancient" Pearl River Estuary and discharged into the paleo-coastal delta in the current outer shelf prior to ∼10 ka cal B.P., creating the relict sediments in the NW Shenhu and NW Dongsha areas. The current outer shelf might have developed as a vast coastal plain under dry and cold conditions at that time.

The line of evidence shows that the sea-level in the NSCS was ∼130 m below the current sea level during the LGM. Following climate warming and the last deglaciation and sea-level rise, the paleo-coastal deltas retreated toward the shore. Zong et al. (2012) and Xiong et al. (2018) suggested that the sea level might have reached the ca. −90 m isobaths around ∼14 ka and ca. −70 m in the early Holocene (e.g., Ge et al., 2014; Zong, 2004). Our in situ shell AMS ^{14}C age data, sedimentological and geochemical signatures for the surface sediments and spatial pattern of the particle size (Table 1 and Figures 2–6) demonstrate that the isobaths of ca. −90 m likely represent the boundary separating the modern sediments from the relicts in the NSCS. As a result, the isobath location roughly corresponds to the last glacial shoreline or the early Holocene coastal delta (e.g., Hanebuth et al., 2000; Lin et al., 2021; Liu et al., 2016; Zong et al., 2012). At ∼7 ka, the sea level reached the maximum elevation and then fell to the modern level in 5.9 ka (e.g., Ge et al., 2014; Stanley & Warne, 1994; Xiong et al., 2018; Zong, 2004; Zong et al., 2012). As a response to the hydrodynamic changes due to the rising sea level, the fine-grained overburden deposited at the last glacial period was continuously removed, finally resulting in the presently-observed relict sands (with less fine-grained components) in the NW Shenhu (Area II) and NW Dongsha (Area III) areas of the NSCS.

5. Conclusion

Numerous sediments accumulated on the current NSSCS were largely exposed during the LGM and potentially reworked in response to the post-glacial sea-level rising and hydrodynamic changes. The unburied sediments deposited during the LGM to earliest Holocene (relict sediments) might be distinct from the alongshore modern-discharged sediments in the depositional environment, benthic organism, and shoreline or delta topography. Revisited the nature of the NSSCS surface sediments is beneficial to the reconstruction of the last glacial shoreline and assessment of the Holocene climate and sea-level changes. A comprehensive analysis is presented in this study for in situ shell AMS ^{14}C dating, and sedimentological and whole-rock geochemical data of the NSCS surface sediments. We detect that the modern sediments are mainly preserved on the NW inner shelf with the Pearl Estuary Channel, which are highly controlled by the Guangdong Longshore Current and the secondary cyclonic eddies. The relict sediments are dominated by well-sorted medium-to coarse-grained sands deposited in a cold and dry environment during the last glacial period. They were mainly preserved in the NW Shenhua and Dongshan areas of the NSCS outer shelf. In the Taiwan Shoal and its surroundings, the LGM-deposited sediments are heavily re-activated due to the compound effect of the modern hydrodynamic environment and terrestrial supply, and post-glacial sea-level rising. Our work reveals that the current ∼−90 m isobaths might be in close proximity to either the last glacial shoreline or the northern boundary of the early Holocene (∼10 ka) coastal delta.

Data Availability Statement

The raw supplementary datasets related to this article are available at https://doi.10.17632/tvvbfp4yr9, open-source online data repository hosted at Mendeley Data.

Acknowledgments
Profs. Amy East and Daan Beelen, and two anonymous reviewers are thanked for their critical comments and constructive suggestions. Drs. X Qiu, X.Q Yu, C.Y Peng, and L.D Zhang are gratefully acknowledged for their field and experimental help. We acknowledge the National Key R&D Program of China (2021YFC3001000), the National Natural Science Foundation of China (U1911204), Innovation Group Project of Southern Marine Science and Engineering Guangdong Lab (Zhuhai) (311022010), Guangdong Introduced Innovative R&D Team Project (2016ZT06N331) and Graduate Quality Improvement Program of Sun Yat-sen University (76140-11230011) for financial supports.

References

Bhatia, M. R., & Taylor, S. R. (1981). Trace-element geochemistry and sedimentary provinces: A study from the Tasman Geosyncline, Australia. *Chemical Geology*, *33*(1–4), 115–125. https://doi.org/10.1016/0009-2541(81)90089-9

Blott, S. J., & Pye, K. (2001). GRADISTAT: A grain size distribution and statistics package for the analysis of unconsolidated sediments. *Earth Surface Processes and Landforms*, *26*(11), 1237–1248. https://doi.org/10.1002/esp.261

Cai, G., Miao, L., Chen, H., Sun, G., Wu, J., & Xu, Y. (2013). Grain size and geochemistry of surface sediments in northwestern continental shelf of the South China Sea. *Environmental Earth Sciences*, *70*(1), 363–380. https://doi.org/10.1007/s12665-012-2133-x

Cao, L., Liu, J., Shi, X., He, W., & Chen, Z. (2019). Source-to-sink processes of fluvial sediments in the northern South China Sea: Constraints from river sediments in the coastal region of South China. *Journal of Asian Earth Sciences*, *185*, 104020. https://doi.org/10.1016/j.jseaes.2019.104020

Carlson, A. E., Stoner, J. S., Donnelly, J. P., & Hillaire-Marcel, C. (2008). Response of the southern Greenland Ice Sheet during the last two deglaciations. *Geology*, *36*(5), 359–362. https://doi.org/10.1130/g24519a.1

Caruso, M. J., Gawarkiewicz, G. G., & Beardsley, R. C. (2006). Inter-annual variability of the Kuroshio intrusion in the South China Sea. *Journal of Oceanography*, *62*(4), 559–575. https://doi.org/10.1007/s10872-006-0076-0

Chappell, J., & Polach, H. (1991). Post-glacial sea-level rise from a coral record at Huon Peninsula, Papua New Guinea. *Nature*, *349*(6305), 147–149. https://doi.org/10.1038/349147a0

Chen, H. (1993). Characteristics and sources of heavy minerals in surface sediment of Taiwan Strait. *Journal of Oceanography in Taiwan Strait*, *12*, 136–144.

Chen, H., Xie, X., Van Rooij, D., Vandorpe, T., Su, M., & Wang, D. (2014). Depositional characteristics and processes of along-slope currents related to a seamount on the northwestern margin of the northwest sub-basin, South China Sea. *Marine Geology*, *355*, 36–53. https://doi.org/10.1016/j.margeo.2014.05.008

Chen, L., Xu, W., Shen, S., & Li, A. (1986). Mineral assemblages and their distribution pattern in the sediments from the north continental shelf of the South China Sea and the Beibu Gulf. *Marine Science*, *10*(3), 6–10.

Chiu, J. K., & Liu, C.-S. (2008). Comparison of sedimentary processes on adjacent passive and active continental margins offshore of SW Taiwan based on echo character studies. *Basin Research*, *20*(4), 503–518. https://doi.org/10.1111/j.1365-2117.2008.00388.x

Chu, P. C., & Guihua, W. (2003). Seasonal variability of thermohaline front in the Central South China Sea. *Journal of Oceanography*, *59*(1), 65–78. https://doi.org/10.1023/a:1022868407012

Chung, Y., Chang, H., & Hung, G. (2004). Particulate flux and ^{210}Pb determined on the sediment trap and core samples from the northern South China Sea. *Continental Shelf Research*, *24*(6), 673–691. https://doi.org/10.1016/j.csr.2004.01.003

Cullers, R. L. (2000). The geochemistry of shales, siltstones and sandstones of Pennsylvanian–Permian age, Colorado, USA: Implications for provenance and metamorphic studies. *Lithos*, *51*(3), 181–203. https://doi.org/10.1016/s0024-4937(99)00063-8

Ding, X., Ye, S., Laws, E. A., Mozdzer, T. J., Yuan, H., Zhao, G., et al. (2019). The concentration distribution and pollution assessment of heavy metals in surface sediments of the Bohai Bay, China. *Marine Pollution Bulletin*, *149*, 110497. https://doi.org/10.1016/j.marpolbul.2019.110497

Dong, L., Su, J., Wong, L. A., Cao, Z., & Chen, J.-C. (2004). Seasonal variation and dynamics of the Pearl River plume. *Continental Shelf Research*, *24*(16), 1761–1777. https://doi.org/10.1016/j.csr.2004.06.006

Emery, K. (1968). Relict sediments on continental shelves of world. *AAPG Bulletin*, *52*(3), 445–464.

Fang, G., Fang, W., Fang, Y., & Wang, K. (1998). A survey of studies on the South China Sea upper ocean circulation. *Acta. Oceanologica Taiwan.*, *37*, 1–16.

Fang, W., Guo, P., Liu, C., Fang, G., & Li, S. (2015). Observed sub-inertial current variability and volume transport over the continental shelf in the northern South China Sea. *Estuarine, Coastal and Shelf Science*, *157*, 19–31. https://doi.org/10.1016/j.ecss.2015.02.001

Fralick, P. W., & Kronberg, B. I. (1997). Geochemical discrimination of clastic sedimentary rock sources. *Sedimentary Geology*, *113*(1), 111–124. https://doi.org/10.1016/S0037-0738(97)00049-3

Gao, X., Chen, S., & Long, A. (2008). Chemical speciation of 12 metals in surface sediments from the northern South China Sea under natural grain size. *Marine Pollution Bulletin*, *56*(4), 786–792. https://doi.org/10.1016/j.marpolbul.2008.01.004

Ge, Q., Liu, J., Xue, Z., & Chu, F. (2014). Dispersal of the Zhujiang River (Pearl River) derived sediment in the Holocene. *Acta Oceanologica Sinica*, *33*(8), 1–9. https://doi.org/10.1007/s13131-014-0407-8

Gong, C., Wang, Y., Xu, S., Pickering, K. T., Peng, X., Li, W., & Yan, Q. (2015). The northeastern South China Sea margin created by the combined action of down-slope and along-slope processes: Processes, products and implications for exploration and paleoceanography. *Marine and Petroleum Geology*, *64*, 233–249. https://doi.org/10.1016/j.marpetgeo.2015.01.016

Hanebuth, T., Stattegger, K., & Grootes, P. M. (2000). Rapid flooding of the Sunda shelf: A late-glacial sea-level record. *Science*, *288*(5468), 1033–1035. https://doi.org/10.1126/science.288.5468.1033

Heaton, T. J., Köhler, P., Butzin, M., Bard, E., Reimer, R. W., Austin, W. E. N., et al. (2020). Marine20—The Marine radiocarbon age calibration curve (0–55,000 cal BP). *Radiocarbon*, *62*(4), 779–820. https://doi.org/10.1017/RDC.2020.68

Hu, B., Li, J., Cui, R., Wei, H., Zhao, J., Li, G., et al. (2014). Clay mineralogy of the riverine sediments of Hainan Island, South China Sea: Implications for weathering and provenance. *Journal of Asian Earth Sciences*, *96*, 84–92. https://doi.org/10.1016/j.jseaes.2014.08.036

Hu, J., Kawamura, H., Hong, H., & Qi, Y. (2000). A review on the currents in the South China Sea: Seasonal circulation, South China Sea warm current and Kuroshio Intrusion. *Journal of Oceanography*, *56*(6), 607–624.

Huh, C. A., Chen, W., Hsu, F. H., Su, C. C., Chiu, J. K., Lin, S., et al. (2011). Modern (<100 years) sedimentation in the Taiwan Strait: Rates and source-to-sink pathways elucidated from radionuclides and particle size distribution. *Continental Shelf Research*, *31*(1), 47–63. https://doi.org/10.1016/j.csr.2010.11.002

Ishizawa, T., Goto, K., Yokoyama, Y., & Goff, J. (2020). Dating tsunami deposits: Present knowledge and challenges. *Earth-Science Reviews*, *200*, 102971. https://doi.org/10.1016/j.earscirev.2019.102971

Jia, J., Wang, C., Su, M., Yan, W., Zeng, L., & Cui, H. (2023). Provenance and dispersal patterns of sediments on the continental shelf of northern South China Sea: Evidence from detrital zircon geochronology. *Marine Geology*, *457*, 107013. https://doi.org/10.1016/j.margeo.2023.107013

Lambeck, K., Rouby, H., Purcell, A., Sun, Y., & Sambridge, M. (2014). Sea level and global ice volumes from the last glacial maximum to the Holocene. *Proceedings of the National Academy of Sciences*, *111*(43), 15296–15303. https://doi.org/10.1073/pnas.1411762111

Li, C., Chen, G., Yao, M., & Wang, P. (1991). The influences of suspended load on the sedimentation in the coastal zones and continental shelves of China. *Marine Geology*, *96*(3–4), 341–352. https://doi.org/10.1016/0025-3227(91)90155-w

Li, C. F., Zhou, Z., Hao, H., Chen, H., Wang, J., Chen, B., & Wu, J. (2008). Late Mesozoic tectonic structure and evolution along the present-day northeastern South China Sea continental margin. *Journal of Asian Earth Sciences*, *31*(4–6), 546–561. https://doi.org/10.1016/j.jseaes.2007.09.004

Li, G., Yan, W., Zhong, L., Xia, Z., & Wang, S. (2015). Provenance of heavy mineral deposits on the northwestern shelf of the South China Sea: Evidence from single-mineral chemistry. *Marine Geology*, *363*, 112–124. https://doi.org/10.1016/j.margeo.2015.01.015

Li, J., Gao, J., Wang, Y., Li, Y., Bai, F., & Cees, L. (2012). Distribution and dispersal pattern of clay minerals in surface sediments, eastern Beibu Gulf, South China Sea. *Acta Oceanologica Sinica*, *31*(2), 78–87. https://doi.org/10.1007/s13131-012-0194-z

Li, L., Clift, P. D., & Nguyen, H. T. (2013). The sedimentary, magmatic and tectonic evolution of the southwestern South China Sea revealed by seismic stratigraphic analysis. *Marine Geophysical Researches*, *34*(3), 341–365. https://doi.org/10.1007/s11001-013-9171-y

Li, L., Switzer, A. D., Chan, C. H., Wang, Y., Weiss, R., & Qiu, Q. (2016). How heterogeneous coseismic slip affects regional probabilistic tsunami hazard assessment: A case study in the South China Sea. *Journal of Geophysical Research: Solid Earth*, *121*(8), 6250–6272. https://doi.org/10.1002/2016jb013111

Li, S., & Gong, C. (2016). Flow dynamics and sedimentation of lateral accretion packages in sinuous deep-water channels: A 3D seismic case study from the northwestern South China Sea margin. *Journal of Asian Earth Sciences*, *124*, 233–246. https://doi.org/10.1016/j.jseaes.2016.05.008

Lin, Y., Hibbert, F. D., Whitehouse, P. L., Woodroffe, S. A., Purcell, A., Shennan, I., & Bradley, S. L. (2021). A reconciled solution of Meltwater Pulse 1A sources using sea-level fingerprinting. *Nature Communications*, *12*(1), 2015. https://doi.org/10.1038/s41467-021-21990-y

Liu, J., Chen, Z., Chen, M., Yan, W., Xiang, R., & Tang, X. (2010). Magnetic susceptibility variations and provenance of surface sediments in the South China Sea. *Sedimentary Geology*, *230*(1–2), 77–85. https://doi.org/10.1016/j.sedgeo.2010.07.001

Liu, J., Clift, P. D., Yan, W., Chen, Z., Chen, H., Xiang, R., & Wang, D. (2014). Modern transport and deposition of settling particles in the northern South China Sea: Sediment trap evidence adjacent to Xisha Trough. *Deep-Sea Research Part I*, *93*, 145–155. https://doi.org/10.1016/j.dsr.2014.08.005

Liu, J., Liu, C., Xu, K., Milliman, J., Chiu, J., Kao, S., & Lin, S. (2008). Flux and fate of small mountainous rivers derived sediments into the Taiwan Strait. *Marine Geology*, *256*(1–4), 65–76. https://doi.org/10.1016/j.margeo.2008.09.007

Liu, J., Xiang, R., Chen, M., Chen, Z., Yan, W., & Liu, F. (2011). Influence of the Kuroshio current intrusion on depositional environment in the northern South China Sea: Evidence from surface sediment records. *Marine Geology*, *285*(1–4), 59–68. https://doi.org/10.1016/j.margeo.2011.05.010

Liu, J., Yan, W., Chen, Z., & Lu, J. (2012). Sediment sources and their contribution along northern coast of the South China Sea: Evidence from clay minerals of surface sediments. *Continental Shelf Research*, *47*, 156–164. https://doi.org/10.1016/j.csr.2012.07.013

Liu, Z., Colin, C., Li, X., Zhao, Y., Tuo, S., Chen, Z., et al. (2010). Clay mineral distribution in surface sediments of the northeastern South China Sea and surrounding fluvial drainage basins: Source and transport. *Marine Geology*, *277*(1–4), 48–60. https://doi.org/10.1016/j.margeo.2010.08.010

Liu, Z., & Stattegger, K. (2014). South China Sea fluvial sediments: An introduction preface. *Journal of Asian Earth Sciences*, *79*, 507–508. https://doi.org/10.1016/j.jseaes.2013.11.003

Liu, Z., Tuo, S., Colin, C., Liu, J. T., Huang, C. Y., Selvaraj, K., et al. (2008). Detrital fine-grained sediment contribution from Taiwan to the northern South China Sea and its relation to regional ocean circulation. *Marine Geology*, *255*(3–4), 149–155. https://doi.org/10.1016/j.margeo.2008.08.003

Liu, Z., Zhao, Y., Colin, C., Siringan, F. P., & Wu, Q. (2009). Chemical weathering in Luzon, Philippines from clay mineralogy and major-element geochemistry of river sediments. *Applied Geochemistry*, *24*(11), 2195–2205. https://doi.org/10.1016/j.apgeochem.2009.09.025

Liu, Z., Zhao, Y., Colin, C., Stattegger, K., Wiesner, M. G., Huh, C. A., et al. (2016). Source-to-sink transport processes of fluvial sediments in the South China Sea. *Earth-Science Reviews*, *153*, 238–273. https://doi.org/10.1016/j.earscirev.2015.08.005

Luan, X., Peng, X., Wang, Y., & Qiu, Y. (2010). Activity and formation of sand waves on northern South China Sea shelf. *Journal of Earth Sciences*, *21*(1), 55–70. https://doi.org/10.1007/s12583-010-0005-4

Lüdmann, T., Wong, H. K., & Wang, P. (2001). Plio-Quaternary sedimentation processes and Neotectonics of the northern continental margin of the South China Sea. *Marine Geology*, *172*(3–4), 331–358. https://doi.org/10.1016/s0025-3227(00)00129-8

Luo, C. X., Zheng, Z., Zou, H. X., Pan, A. D., Fang, G., Bai, J. J., et al. (2013). Palaeoenvironmental significance of grain-size distribution of river flood deposits: A study of the archaeological sites of the Apengjiang River drainage, upper Yangtze region, Chongqing, China. *Journal of Archaeological Science*, *40*(2), 827–840. https://doi.org/10.1016/j.jas.2012.09.020

Ma, D., & Liu, X. (1994). The formation and development of Taiwan Shoal. *Marine Geological Letters*, *07*, 4–6.

McLennan, S. M., Taylor, S. R., McCulloch, M. T., & Maynard, J. B. (1990). Geochemical and Nd Sr isotopic composition of deep-sea turbidites: Crustal evolution and plate tectonic associations. *Geochimica et Cosmochimica Acta*, *54*(7), 2015–2050. https://doi.org/10.1016/0016-7037(90)90269-Q

McManus, D. A. (1975). Modern versus relict sediment on the continental shelf. *Geological Society of America Bulletin*, *86*(8), 1154–1160. https://doi.org/10.1130/0016-7606(1975)86<1154:mvrsot>2.0.co;2

Milliman, J. D., & Farnsworth, K. L. (2011). *River discharge to the coastal ocean: A global synthesis*. Cambridge University Press.

Nesbitt, H. W., Markovics, G., & Price, R. C. (1980). Chemical processes affecting alkalis and alkaline Earth during continental weathering. *Geochimica et Cosmochimica Acta*, *44*(11), 1659–1666. https://doi.org/10.1016/0016-7037(80)90218-5

Niino, H., & Emery, K. O. (1961). Sediments of shallow portions of East China Sea and South China Sea. *Geological Society of America Bulletin*, *72*(5), 731–762. https://doi.org/10.1130/0016-7606(1961)72[731:sospoe]2.0.co;2

Orme, G. R. (1982). Relict sediment. In *Beaches and coastal geology. Encyclopedia of Earth sciences series*. Springer. https://doi.org/10.1007/0-387-30843-1362

Pan, X., Wong, G. T. F., Tai, J. H., & Ho, T. Y. (2015). Climatology of physical hydrographic and biological characteristics of the Northern South China Sea Shelf-sea (NoSoCS) and adjacent waters: Observations from satellite remote sensing. *Deep-Sea Research Part II*, *117*, 10–22. https://doi.org/10.1016/j.dsr2.2015.02.022

Papista, E., Dimitrakis, D., & Yiantsios, S. (2011). Direct numerical simulation of incipient sediment motion and hydraulic conveying. *Industrial & Engineering Chemistry Research*, *50*(2), 630–638. https://doi.org/10.1021/ie1000828

Qu, T., Kim, Y. Y., Yaremchuk, M., Tozuka, T., Ishida, A., & Yamagata, T. (2004). Can Luzon Strait transport play a role in conveying the impact of ENSO to the South China Sea? *Journal of Climate*, *17*(18), 3644–3657. https://doi.org/10.1175/1520-0442(2004)017<3644:clstpa>2.0.co;2

Reeder, D. B., Ma, B. B., & Yang, Y. J. (2011). Very large subaqueous sand dunes on the upper continental slope in the South China Sea generated by episodic, shoaling deep-water internal solitary waves. *Marine Geology*, *279*(1–4), 12–18. https://doi.org/10.1016/j.margeo.2010.10.009

Schlee, J. (1968). Sand and gravel on the continental shelf off the Northeastern United States. *Journal of Mental Science*, *95*(400), 319–382.

Shao, L., Li, X., Geng, J., Pang, X., Lei, Y., Qiao, P., et al. (2007). Deep water bottom current deposition in the northern South China Sea. *Science in China, Series AD*, *50*(7), 1060–1066. https://doi.org/10.1007/s11430-007-0015-y

Shaw, P. T., & Chao, S. Y. (1994). Surface circulation in the South China sea. *Deep-Sea Research Part I*, *41*(11–12), 1663–1683. https://doi.org/10.1016/0967-0637(94)90067-1

Shen, X., Jian, X., Li, C., Liu, J. T., Chang, Y.-P., Zhang, S., et al. (2021). Submarine topography-related spatial variability of the southern Taiwan Strait sands (East Asia). *Marine Geology*, *436*, 106495. https://doi.org/10.1016/j.margeo.2021.106495

Singh, S. K., Sarin, M., & France-Lanord, C. (2005). Chemical erosion in the eastern Himalaya: Major ion composition of the Brahmaputra and $\delta^{13}C$ of dissolved inorganic carbon. *Geochimica et Cosmochimica Acta*, *69*(14), 3573–3588. https://doi.org/10.1016/j.gca.2005.02.033

Stanley, D. J., & Warne, A. G. (1994). Worldwide initiation of Holocene marine deltas by deceleration of sea-level rise. *Science*, *265*(5169), 228–231. https://doi.org/10.1126/science.265.5169.228

Stuiver, M., Reimer, P. J., & Braziunas, T. F. (1998). High-precision radiocarbon age calibration for terrestrial and marine samples. *Radiocarbon*, *40*(3), 1127–1151. https://doi.org/10.1017/s0033822200019172

Su, J. (2004). Overview of the South China Sea circulation and its influence on the coastal physical oceanography outside the Pearl River Estuary. *Continental Shelf Research*, *24*(16), 1745–1760. https://doi.org/10.1016/j.csr.2004.06.005

Su, J., & Pohlmann, T. (2009). Wind and topography influence on an upwelling system at the eastern Hainan coast. *Journal of Geophysical Research*, *114*(C6), C06017. https://doi.org/10.1029/2008jc005018

Swift, J. P. D., Stanley, D. J., & Curray, J. R. (1971). Relict Sediments on continental shelves: A Reconsideration. *The Journal of Geology*, *79*(3), 322–346. https://doi.org/10.1086/627629

Switzer, A. D., & Pile, J. (2015). Grain size analysis: Handbook of sea-level research (pp. 331–346).

Tamburini, F., Adatte, T., Föllmi, K., Bernasconi, S. M., & Steinmann, P. (2003). Investigating the history of East Asian monsoon and climate during the last glacial–interglacial period (0–140 000 years): Mineralogy and geochemistry of ODP sites 1143 and 1144, South China Sea. *Marine Geology*, *201*(1–3), 147–168. https://doi.org/10.1016/s0025-3227(03)00214-7

Tan, Q., & Sun, Y. (1988). *Littoral placer deposits in China*. Science Press. (In Chinese).

Wang, G., Xie, S., Qu, T., & Rui, X. H. (2011). Deep South China Sea circulation. *Geophysical Research Letters*, *38*(5). https://doi.org/10.1029/2010gl046626

Wang, P. (1999). Response of Western Pacific marginal seas to glacial cycles: Paleoceanographic and sedimentological features. *Marine Geology*, *156*(1–4), 5–39. https://doi.org/10.1016/s0025-3227(98)00172-8

Wang, P., Du, Y., Yu, W., Algeo, T. J., Zhou, Q., Xu, Y., et al. (2020). The chemical index of alteration (CIA) as a proxy for climate change during glacial-interglacial transitions in Earth history. *Earth-Science Reviews*, *201*, 103032. https://doi.org/10.1016/j.earscirev.2019.103032

Wang, P., & Li, Q. (2009). *The South China Sea: Paleoceanography and sedimentology*. Springer Nature.

Wang, Y., Ren, M. E., & Zhu, D. (1986). Sediment supply to the continental shelf by the major rivers of China. *Journal of the Geological Society*, *143*(6), 935–944. https://doi.org/10.1144/gsjgs.143.6.0935

Wang, Y., Wang, Y., Chen, X., & Zhang, L. (2022). Source-to-sink process and risk assessment of heavy metals for the surface sediment in the northern South China Sea. *Environmental Science & Pollution Research*, *30*(2), 1–19. https://doi.org/10.1007/s11356-022-22281-9

Webster, P. J., & Peter, J. (1994). The role of hydrological processes in ocean-atmosphere interactions. *Review of Geophysics*, *32*(4), 427–476. https://doi.org/10.1029/94rg01873

Wehausen, R., & Brumsack, H. J. (2002). Astronomical forcing of the East Asian monsoon mirrored by the composition of Pliocene South China Sea sediments. *Earth and Planetary Science Letters*, *201*(3–4), 621–636. https://doi.org/10.1016/s0012-821x(02)00746-x

Wronkiewicz, D. J., & Condie, K. C. (1987). Geochemistry of Archean Shales from the Witwatersrand Supergroup, South Africa: 421. Source area weathering and provenance. *Geochimica et Cosmochimica Acta*, *51*(9), 2401–2416. https://doi.org/10.1016/0016-7037(87)90293-6

Xiong, H., Zong, Y., Qian, P., Huang, G., & Fu, S. (2018). Holocene sea-level history of the northern coast of South China Sea. *Quaternary Science Reviews: International Multidisciplinary Research Journal*, *194*, 12–26. https://doi.org/10.1016/j.quascirev.2018.06.022

Xu, F., Tian, X., Yin, F., Zhao, Y., & Yin, X. (2016). Heavy metals in the surface sediments of the northern portion of the South China Sea shelf: Distribution, contamination, and sources. *Environmental Science and Pollution Research International*, *23*(9), 8940–8950. https://doi.org/10.1007/s11356-016-6151-1

Yang, H. N., Chen, Z., Yan, W., Gu, S. C., & Wu, B. H. (2005). *Solid mineral resources in South China Sea and the distribution. Marine geology of China offshore and mineral resources*. Ocean Press. (In Chinese).

Yang, S., Yim, W. W. S., & Huang, G. (2008). Geochemical composition of inner shelf quaternary sediments in the northern South China Sea with implications for provenance discrimination and paleo-environmental reconstruction. *Global and Planetary Change*, *60*(3–4), 207–221. https://doi.org/10.1016/j.gloplacha.2007.02.005

Yim, W. S., Huang, G., Fontugne, M., Hale, R. E., Paterne, M., Pirazzoli, P. A., & Ridley Thomas, W. (2006). Post-glacial sea-level changes in the northern South China Sea continental shelf: Evidence for a post-8200 cal BP melt-water pulse. *Quaternary International*, *145–146*, 55–67. https://doi.org/10.1016/j.quaint.2005.07.005

Yu, H. S., & Song, G. S. (2000). Submarine physiographic features in Taiwan region and their geological significance. *Journal of the Geological Society of China*, *43*, 267–286.

Yuan, D., Han, W., & Hu, D. (2006). Surface Kuroshio path in the Luzon Strait area derived from satellite remote sensing data. *Journal of Geophysical Research*, *111*(C11), C11007. https://doi.org/10.1029/2005jc003412

Zhang, J., Wang, D. R., Jennerjahn, T., & Dsikowitzky, L. (2013). Land-sea interactions at the east coast of Hainan Island, South China Sea: A synthesis. *Continental Shelf Research*, *57*, 132–142. https://doi.org/10.1016/j.csr.2013.01.004

Zhang, W., Wei, X., Zheng, J., Zhu, Y., & Zhang, Y. (2012). Estimating suspended sediment loads in the Pearl River Delta region using sediment rating curves. *Continental Shelf Research*, *38*, 35–46. https://doi.org/10.1016/j.csr.2012.02.017

Zhang, Z. Y., Chen, H. T., Liu, R. H., & Huang, S. H. (1992). *Quaternary littoral placer in South China*. Geologic Press. (In Chinese).

Zhao, D., Wan, S., Yu, Z., & Huang, J. (2015). Distribution, enrichment and sources of heavy metals in surface sediments of Hainan Island rivers, China. *Environmental Earth Sciences*, *74*(6), 1–14. https://doi.org/10.1007/s12665-015-4522-4

Zhong, L., Li, G., Yan, W., Xia, B., Feng, Y., Miao, L., & Zhao, J. (2017). Using zircon U–Pb ages to constrain the provenance and transport of heavy minerals within the northwestern shelf of the South China Sea. *Journal of Asian Earth Sciences*, *134*, 176–190. https://doi.org/10.1016/j.jseaes.2016.11.019

Zhong, Y., Chen, Z., Li, L., Liu, J., Li, G., Zheng, X., et al. (2017). Bottom water hydrodynamic provinces and transport patterns of the northern South China Sea: Evidence from grain size of the terrigenous sediments. *Continental Shelf Research*, *140*, 11–26. https://doi.org/10.1016/j.csr.2017.01.023

Zhu, M., Graham, S., Xiong, P., & Mchargue, T. (2010). Characteristics of migrating submarine canyons from the middle Miocene to present: Implications for paleoceanographic circulation, northern South China Sea. *Marine and Petroleum Geology*, *27*(1), 307–319. https://doi.org/10.1016/j.marpetgeo.2009.05.005

Zong, Y. (2004). Mid-Holocene sea-level highstand along the Southeast Coast of China. *Quaternary International*, *117*(1), 55–67. https://doi.org/10.1016/s1040-6182(03)00116-2

Zong, Y., Huang, K., Yu, F., Zhuo, Z., Switzer, A., Huang, G., et al. (2012). The role of sea-level rise, monsoonal discharge and the Paleo-landscape in the early Holocene evolution of the Pearl River Delta, southern China. *Quaternary Science Reviews*, *54*, 77–88. https://doi.org/10.1016/j.quascirev.2012.01.002